

SI Text

SI Materials and Methods

Bacterial strains, plasmids, and growth conditions. Bacterial strains and plasmids used in this study are listed in SI Table 2. *Salmonella enterica* serovar Typhimurium strains are derived from the wild-type strain 14028s. Phage P22-mediated transductions were performed as described (1). Bacteria were typically grown at 37°C in LB broth (2) or in N-minimal medium at pH 7.7 (3) supplemented with 0.1 % Casamino Acids, 38 mM glycerol, 20 μ M or 10 mM MgCl_2 , and 100 μ M FeCl_3 . Lac^+ colonies were selected on N-minimal medium at pH 7.7 supplemented with 38 mM lactose, 10 μ M MgCl_2 . Counterselections for tetracycline-sensitive (Tet^s) colonies were performed as described (4). Ampicillin and kanamycin were used at 50 μ g/ml, tetracycline at 12.5 μ g/ml and chloramphenicol at 20 μ g/ml.

Construction of chromosomal mutants. Strain EG17235, which has a *tetRA* insertion in the *pbgP* promoter region, was constructed by the one-step gene inactivation method (5). The *tetRA* genes were amplified using primers 6105 and 6106 and plasmid pEG5342 harboring the transposon Tn10 as template and recombined into the *pbgP* promoter region of the wild-type 14028s strain.

Strain EG17242, which has a synthetic PhoP box instead of the original PmrA box at the *pbgP* promoter, was constructed by a combination of the one-step gene inactivation method and counter selection method for Tet^s colonies. A primer

partial homoduplex containing the synthetic PhoP box was generated using primers 6107 and 6108 and recombined into the chromosome, replacing the *tetRA* gene at the *pbgP* promoter region in strain EG17235.

Strain EG17236, which has a *tetRA* insertion in the *ugd* promoter region, was constructed by the one-step gene inactivation method. The *tetRA* genes were amplified using primers 6111 and 6112 and plasmid pEG5342 harboring the transposon Tn10 as template and recombined into the *ugd* promoter region in the wild-type 14028s strain.

Strain EG17238, which has a Cm^R cassette downstream of the *tetA* gene in the *ugd* promoter region, was constructed by the one-step gene inactivation method. The Cm^R cassette was amplified using primers 6245 and 6255 and pKD3 as template, and recombined into the *pbgP* promoter region of the EG17236 strain.

Strain EG17243, which has a synthetic PhoP box instead of the original PmrA box at the *ugd* promoter, was constructed by a combination of the one-step gene inactivation method and counter selection method for Tet^s colonies. A primer partial homoduplex containing the synthetic PhoP box was generated using primers 6113 and 6114 and recombined into the chromosome, replacing the *tetRA* gene at the *ugd* promoter region in the strain EG17238.

All strains constructed by using PCRs were analyzed by DNA sequencing and confirmed that the DNA regions generated by PCR had the predicted sequences and no unexpected substitutions. Primers used in the construction of chromosomal mutants are listed in SI Table 3.

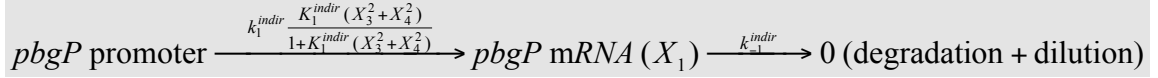
Degradation rate analysis by quantitative Western blotting. Bacteria were grown as described above, in 25 ml media of low Mg²⁺ culture for 2 h; then,

chloramphenicol (200 $\mu\text{g}/\text{ml}$) was added to inhibit protein synthesis. A 1-ml aliquot of bacterial cell culture was collected at the indicated time points, mixed immediately with 1/5 volume of 5% phenol pH 4.3 (Sigma)/95% ethanol to inactivate cellular proteases, and kept on ice for at least 30 min. After spinning down, cells were resuspended in an appropriate volume of B-PER solution (Pierce). A whole-cell lysate (10 μg of protein) was run on a Bis-Tris 10% gel (Invitrogen) with MES SDS Running buffer, transferred to a PVDF membrane, and analyzed by Western blots using anti-PmrD polyclonal antibodies. Western blots were developed by using anti-rabbit IgG horseradish peroxidase-linked antibodies (Amersham Biosciences) and Supersignal west femto (Pierce). Protein levels were digitized and quantified by using a film developed for Western blot, a fluorescence plate, and an FLA-5000 imaging system (Fuji Film).

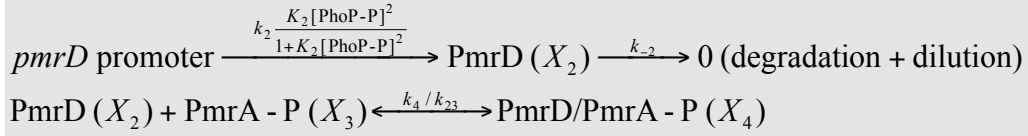
Description and Derivation of the Mathematical Models

Our mathematical models for the direct and connector-mediated pathway dynamics describe temporal changes in the concentration of the *pbgP* mRNA. Because it is known that the rRNA concentration does not change when bacteria are growing at a constant rate (see, e. g., ref. 6), our models also describe the dynamics of the *pbgP* mRNA concentration relative to that of 16S rRNA, and can be fitted to the experimental data presented in Fig. 3A. The ODEs (ordinary differential equations) constituting the model of the connector-mediated transcription control circuit are given below (under each equation, in gray boxes, we list the corresponding chemical reactions):

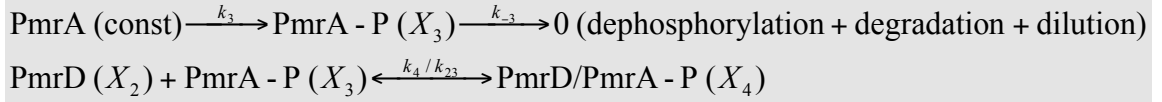
$$\frac{dX_1}{dt} = k_1^{indir} \frac{K_1^{indir} (X_3^2 + X_4^2)}{1 + K_1^{indir} (X_3^2 + X_4^2)} - k_{-1}^{indir} X_1 ; \quad [1]$$



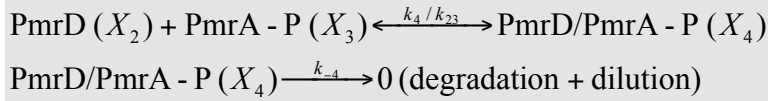
$$\frac{dX_2}{dt} = k_2 \frac{K_2 [\text{PhoP} - \text{P}]^2}{1 + K_2 [\text{PhoP} - \text{P}]^2} + k_{23} X_4 - k_{-2} X_2 - k_4 X_2 X_3 ; \quad [2]$$



$$\frac{dX_3}{dt} = k_3 + k_{23} X_4 - k_{-3} X_3 - k_4 X_2 X_3 ; \quad [3]$$



$$\frac{dX_4}{dt} = k_4 X_2 X_3 - (k_{23} + k_{-4}) X_4 . \quad [4]$$



The correspondence between the concentration variables X_i and the chemical species is as follows: $X_1 \sim pbgP$ mRNA; $X_2 \sim \text{PmrD}$ (protein); $X_3 \sim \text{PmrA-P}$ (phosphorylated protein); $X_4 \sim \text{PmrA-P/PmrD}$ (protein complex).

In Eqs. 1–4, it is assumed that PmrA-P and PmrA-P/PmrD interact with DNA only as homodimers $(\text{PmrA-P})_2$ and $(\text{PmrA-P/PmrD})_2$. We also considered the situation when functional heterodimers can form (see *Model fitting* below);

this situation is described by a system consisting of SI Eqs. 2–4, and SI Eq. 1 modified as follows:

$$\frac{dX_1}{dt} = k_1^{indir} \frac{K_1^{indir} (X_3^2 + X_4^2 + X_3X_4)}{1 + K_1^{indir} (X_3^2 + X_4^2 + X_3X_4)} - k_{-1}^{indir} X_1 \quad [5]$$

The concentration of PhoP-P, which appears in SI Eq. 2, is the external variable representing the input of the transcription control system. The output of the system is the concentration of the *pbgP* mRNA (X_1). In the above equations, the constant k_1^{indir} represents the transcription rate for the *pbgP* inducible promoter (under full induction conditions), and the constant k_2 is the production rate for PmrD (for a fully induced *pmrD* gene). The constants k_{-1}^{indir} and k_{-2} are the rates of exponential depletion (due to biochemical degradation and dilution resulting from cell growth) of *pbgP* mRNA and the PmrD protein, respectively. The constants k_3 and k_{-3} are the production and depletion rates for PmrA-P; k_4 and k_{23} are the forward and backward rates of the reaction PmrD+PmrA-P \leftrightarrow PmrD/PmrA-P. k_{-4} is the rate of exponential depletion of PmrA-P due to protein degradation and dilution. The constants K_1^{indir} and K_2 are the affinities (association constants) for PmrA-P binding to the *pbgP* promoter and PhoP-P binding to the *pmrD* promoter, respectively. In the above model, we assume that only phosphorylated regulator proteins activate transcription (7-9), and that they interact with the corresponding binding sites in the form of dimers (9, 10). The latter assumption is supported by the facts that the PhoP and PmrA proteins recognize distinct tandem repeats in promoters (9, 11).

The dynamic equation for the direct regulation circuit is

$$\frac{dX_1}{dt} = k_1^{dir} \frac{K_1^{dir} [\text{PhoP} - \text{P}]^2}{1 + K_1^{dir} [\text{PhoP} - \text{P}]^2} - k_{-1}^{dir} X_1. \quad [6]$$

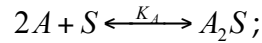
Here, K_1^{dir} is the affinity of PhoP-P binding to the *pbgP* promoter; k_1^{dir} and k_{-1}^{dir} are analogous to k_1^{indir} and k_{-1}^{indir} .

The expressions for the first- and second-order terms on the right-hand sides of the model equations SI Eqs. 1–6 follow directly from our description of the regulatory circuits. In the models, we focus only on the major components and neglect intermediate stages of reactions. It is assumed that the concentrations of all the chemical substances not explicitly presented in the model stay constant (e.g., $[\text{PmrA}] = \text{const}$, and the phosphorylation of PmrA occurs at a constant rate). To simplify the connector-mediated pathway model, we do not include the variable describing changes in the concentration of *pmrD* mRNA. Taking the approach described in the literature (12-15), we assume that the rate of PmrD production is proportional to the activity of the *pmrD* promoter. We also neglect the *pmrD* transcription repression by PmrA-P, because this effect is known to be relatively weak (16). Our description of transcription, translation, and mRNA decay processes as simple zero- and first-order reactions is a simplification justified by our purpose to consider only the most essential parts of the expression control systems.

The approach we used to model transcriptional control is as follows: we assume that two activators, A and B , can competitively bind to DNA binding sites, S , with affinities K_A and K_B , respectively; that the activators bind DNA as dimers; and that each binding site is attached to a promoter. We denote by r the rate of transcription (micromoles/liter of transcripts initiated per minute)

assuming all binding sites are occupied; in reality, only a fraction, $p \in [0, 1]$, of all activator sites are bound. We assume that transcription initiation is possible only for promoters bound to activator proteins. Therefore, the general expression for the transcription initiation rate is pr . Our objective is to find an expression for p in terms of the concentrations of the activator proteins.

The activator protein A binds to the activator site as a result of the reaction



the binding reaction for B is similar (while this reaction is a simplification of reality, we assume that the AS form (bound monomers) never accumulates significantly; as a consequence, the equilibrium equations for more detailed binding mechanisms are well approximated by the one for the reaction above (17)). It can be assumed that the binding reactions are in equilibrium at all times because protein–DNA binding is much faster than other reactions in the system (transcription, translation, phosphorylation). Therefore, the concentrations of the reacting species satisfy the equations

$$K_A = \frac{[A_2S]}{[A]^2[S]}, \quad K_B = \frac{[B_2S]}{[B]^2[S]}$$

Using these equations, we obtain

$$p = \frac{[\text{Bound } S]}{[\text{Total } S]} = \frac{[A_2S] + [B_2S]}{[S] + [A_2S] + [B_2S]} = \frac{K_A[A]^2 + K_B[B]^2}{1 + K_A[A]^2 + K_B[B]^2}.$$

If there exists a positive K such that $K_A \approx K_B \approx K$, we can use the approximation

$$p = \frac{[\text{Bound } S]}{[\text{Total } S]} = \frac{K([A]^2 + [B]^2)}{1 + K([A]^2 + [B]^2)}.$$

This expression is used to model competitive binding of PmrD/PmrA-P and PmrA-P to the binding sites upstream of the *pbgP* promoter (16) in the connector-mediated regulation model (SI Eq. 1). The use of the relation $K_A \approx K_B \approx K$ is justified by our assumption that PmrD/PmrA-P and PmrA-P have approximately the same DNA binding properties. We also postulate that the concentration of free binding proteins is considerably larger than the concentration of binding sites, which is valid because the bacterial cell normally has only one copy of a gene, but hundreds or even thousands (18) of copies of regulator proteins. This postulation allows us to disregard changes in the concentrations of free proteins (and complexes thereof) resulting from the formation of protein–DNA complexes, and thus ignore the details of the binding mechanism.

If in the regulation model described above we consider only one activator protein, then we will arrive at the expression for transcription control by PhoP-P which was used in SI Eqs. 2 and 6. If we consider the possibility of DNA binding by the heterodimers AB , then we will obtain the expression used in SI Eq. 5.

Steady-State Equations and Induction Ratios

The steady-state equations for the models are obtained from SI Eqs. 1–6 by setting the time derivatives to 0. SI Eq. 6 for the direct regulation model has a unique solution:

$$X_1^{dir} = \frac{k_1^{dir}}{k_{-1}^{dir}} \frac{K_1^{dir} [\text{PhoP} - \text{P}]^2}{1 + K_1^{dir} [\text{PhoP} - \text{P}]^2}. \quad [7]$$

The solution to SI Eqs. 1–4 can be found by solving SI Eqs. 2–4 and then substituting the solution into the steady-state version of SI Eq. 1. The resulting steady-state expression for the *pbgP* mRNA concentration reads:

$$X_1^{indir} = \frac{k_1^{indir}}{k_{-1}^{indir}} \frac{K_1^{indir} (X_3^2([\text{PhoP} - \text{P}]) + X_4^2([\text{PhoP} - \text{P}]))}{1 + K_1^{indir} (X_3^2([\text{PhoP} - \text{P}]) + X_4^2([\text{PhoP} - \text{P}]))}. \quad [8]$$

For $X_1([\text{PhoP} - \text{P}])$, the steady-state concentration of *pbgP* mRNA, the induction ratio is defined as $X_1([\text{PhoP} - \text{P}]) / X_1(P_0)$, where P_0 is the concentration of PhoP-P under repressing conditions ($P_0 \ll [\text{PhoP} - \text{P}]$). From this definition and SI Eqs. 7–8 it follows that, for both direct and connector-mediated regulation models, the induction ratio does not depend on k_1 and k_{-1} . The rate constant k_1 reflects the activity of the *pbgP* promoter, therefore, the models predict insensitivity of the induction ratios to variations in *pbgP* promoter activity for both direct and PmrD-mediated control circuits.

A characteristic feature of the induction ratio curves corresponding to the experimental data is that they approach a plateau for ratios greater than 10 (Fig. 2B). However, the curves for the corresponding models do not show this property (Fig. 3B). Such a discrepancy can be explained as follows. The steady-state induction ratio $I([\text{Mg}^{2+}])$ can be represented as a composition of functions: $I([\text{Mg}^{2+}]) = f(g([\text{Mg}^{2+}]))$, where $g([\text{Mg}^{2+}]) = [\text{PhoP} - \text{P}]$. Fig. 2B shows the functions $I([\text{Mg}^{2+}])$, whereas Fig. 3B shows the functions $f([\text{PhoP} - \text{P}])$. Approaching a plateau is equivalent to having small absolute derivative $|I'([\text{Mg}^{2+}])|$; using the chain rule for differentiation, we obtain

$$|I'([\text{Mg}^{2+}])| = |f'(g([\text{Mg}^{2+}]))| |g'([\text{Mg}^{2+}])|.$$

When $[\text{Mg}^{2+}]$ is low, the system approaches its maximum capacity to generate PhoP-P, therefore, $g([\text{Mg}^{2+}])$ should reach a plateau for low $[\text{Mg}^{2+}]$. This assertion is supported by modeling (19). This implies that for low $[\text{Mg}^{2+}]$, $|g'([\text{Mg}^{2+}]|)$ is quite close to 0, and so is $|l'([\text{Mg}^{2+}]|)$, although $|f'(g([\text{Mg}^{2+}]|))|$ is not.

Cascade-Like Properties of the Connector-Mediated Pathway

As a result of model fitting for the connector-mediated pathway, we obtained a parameter set such that $k_4 \gg k_{-4}$ (the PmrA-P/PmrD complex formation rate is significantly larger than the complex degradation/dilution rate, SI Table 5). Therefore, we can simplify the steady-state equations for the PmrD-mediated control circuit by dividing the equations by k_4 and using the approximate equality $k_{-4}/k_4 \approx 0$. With the notation $c_i = k_i/k_4$ for the coefficients, the simplified system of equations reads:

$$c_1^{indir} \frac{K_1^{indir} (X_3^2 + X_4^2)}{1 + K_1^{indir} (X_3^2 + X_4^2)} - c_{-1}^{indir} X_1 = 0;$$

$$c_2 \frac{K_2[\text{PhoP-P}]^2}{1 + K_2[\text{PhoP-P}]^2} + c_{23} X_4 - c_{-2} X_2 - c_4 X_2 X_3 = 0;$$

$$c_3 + c_{23} X_4 - c_{-3} X_3 - c_4 X_2 X_3 = 0;$$

$$c_4 X_2 X_3 - c_{23} X_4 = 0.$$

Using the property $c_i/c_j = k_i/k_j$, we can find the system's unique solution:

$$X_1^{indir} = \frac{k_1^{indir}}{k_{-1}^{indir}} \frac{K_1^{indir} (X_3^2 + X_4^2)}{1 + K_1^{indir} (X_3^2 + X_4^2)}; \quad [9]$$

$$X_2 = \frac{k_2}{k_{-2}} \frac{K_2[\text{PhoP} - \text{P}]^2}{1 + K_2[\text{PhoP} - \text{P}]^2}; \quad [10]$$

$$X_3 = \frac{k_3}{k_{-3}}; \quad [11]$$

$$X_4 = \frac{k_4}{k_{23}} X_2 X_3. \quad [12]$$

For the interval of [PhoP-P] concentrations presented in Fig. 3B, $K_2[\text{PhoP} - \text{P}]^2 < 1$ (SI Table 5). Applying the asymptotic formula $a/(1+a) = a - a^2 + o(a^2)$ to SI Eq. 10 and neglecting the small terms $O(K_2^2[\text{PhoP} - \text{P}]^4)$, from SI Eqs. 10–12 we obtain

$$X_4 \approx AK_2[\text{PhoP} - \text{P}]^2, \quad A = \frac{k_4}{k_{23}} \frac{k_3}{k_{-3}} \frac{k_2}{k_{-2}}.$$

Plugging this expression into SI Eq. 9, we arrive at the simplified equation

$$X_1^{indir} = \frac{k_1^{indir}}{k_{-1}^{indir}} \frac{K_1^{indir} \{(k_3/k_{-3})^2 + A^2 K_2^2 [\text{PhoP} - \text{P}]^4\}}{1 + K_1^{indir} \{(k_3/k_{-3})^2 + A^2 K_2^2 [\text{PhoP} - \text{P}]^4\}}. \quad [13]$$

For the fitted model, $k_3/k_{-3} = 0.002$ (SI Table 5), so we can neglect the term $O(k_3^2/k_{-3}^2)$ and simplify even further:

$$X_1^{indir} = \frac{k_1^{indir}}{k_{-1}^{indir}} \frac{K_1^{indir} A^2 K_2^2 [\text{PhoP} - \text{P}]^4}{1 + K_1^{indir} A^2 K_2^2 [\text{PhoP} - \text{P}]^4}. \quad [14]$$

For any K_2 , SI Eqs. 13 and 14 are valid for sufficiently small [PhoP - P]. SI Eq. 14 is a Hill equation with Hill coefficient 4, whereas SI Eq. 7 for the direct regulation circuit is a Hill equation with Hill coefficient 2 (for a discussion of Hill equations and their properties, see refs. 20-22). The increase in the Hill coefficient (compared to direct regulation) can be attributed to the presence of two stages of

transcriptional regulation in the connector-mediated pathway, and is a rather general property of multi-stage regulatory cascades whose stages have sigmoidal signal–response curves (23).

Let

$$I^{dir}([\text{PhoP} - \text{P}]) = \frac{X_1^{dir}([\text{PhoP} - \text{P}])}{X_1^{dir}(P_0)}, \quad I^{indir}([\text{PhoP} - \text{P}]) = \frac{X_1^{indir}([\text{PhoP} - \text{P}])}{X_1^{indir}(P_0)}$$

be the induction ratios for the direct and connector-mediated pathways (as in *Steady-State Equations and Induction Ratios* above, $P_0 \ll [\text{PhoP} - \text{P}]$ is the concentration of PhoP-P under repressing conditions). It follows from SI Eqs. 7 and 9–12 that, if k_4 (the PmrD/PmrA-P complex formation rate) is large enough (which is true for our fitted model),

$$\lim_{[\text{PhoP} - \text{P}] \rightarrow \infty} \frac{I^{indir}([\text{PhoP} - \text{P}])}{I^{dir}([\text{PhoP} - \text{P}])} \approx \frac{X_1^{dir}(P_0)}{X_1^{indir}(P_0)}. \quad [15]$$

From SI Eq. 13 we have

$$\frac{X_1^{indir}([\text{PhoP} - \text{P}])}{X_1^{dir}([\text{PhoP} - \text{P}])} = O([\text{PhoP} - \text{P}]^2) + O\left(\frac{(k_3/k_{-3})^2}{([\text{PhoP} - \text{P}]^2)}\right) \quad \text{as} \quad [\text{PhoP} - \text{P}] \rightarrow 0. \quad [16]$$

Consequently, if P_0 is small enough and $O((k_3/k_{-3})^2/P_0^2)$ is negligible compared to $O(P_0^2)$, then $X_1^{dir}(P_0)/X_1^{indir}(P_0)$ is large ($\gg 1$). In this case, SI Eq. 15 gives

$$\lim_{[\text{PhoP} - \text{P}] \rightarrow \infty} \frac{I^{indir}([\text{PhoP} - \text{P}])}{I^{dir}([\text{PhoP} - \text{P}])} > 1, \quad [17]$$

meaning that there exists a concentration of PhoP-P, $\tilde{P} \in [P_0, \infty)$, such that

$$I^{indir}(\tilde{P}) = I^{dir}(\tilde{P}), \quad I^{indir}([\text{PhoP} - \text{P}]) > I^{dir}([\text{PhoP} - \text{P}]) \quad \text{for all} \quad [\text{PhoP} - \text{P}] > \tilde{P}.$$

In principle, we can choose different high values of $[\text{Mg}^{2+}]$ (and, therefore, different small values of $[\text{PhoP-P}]$) to represent repressing conditions, $P_0 = P_0([\text{Mg}^{2+}])$. For some choices of P_0 , we will have $\tilde{P} = P_0$ (such as in Fig. 3B); for other choices, we may have $\tilde{P} > P_0$. It should be noted that, because in reality $k_3/k_{-3} > 0$, for vanishingly small $[\text{PhoP-P}]$, the terms $O((k_3/k_{-3})^2/[\text{PhoP-P}]^2)$ cannot be neglected and SI Eq. 17 will not hold. However, the use of vanishingly small P_0 is not biologically meaningful.

Computational Procedures

Dynamics and steady-state computations. The model trajectories in Fig. 3A were generated using MATLAB's SimBiology function `sbiosimulate`. The steady-state solutions for the direct regulation model were computed using SI Eq. 7. The steady states for the connector-mediated pathway were found as follows. First, the steady-state versions of SI Eqs. 2–4 were reduced to a quadratic equation in X_4 , which was solved using MATLAB's `roots` function. If the solution produced one positive root (or two positive roots very close to each other) such that the resulting X_2 and X_3 were also positive, then these values were used to find X_1 (from the steady-state version of SI Eq. 1). If it did not, the steady state was found by solving SI Eqs. 1–4 (using MATLAB's function `ode15s`) on increasing time intervals until convergence, similarly to the way described in (24).

Model fitting. Model fitting with models defined by SI Eqs. 1–4 and SI Eq. 6 was performed as described in *Materials and Methods* of the main article; the fitting results are shown in Fig. 3A, and the resulting parameter sets are given in SI Tables 5 and 6. The data on relative PhoP-P levels for pathway activation were taken from ref. 25 and normalized so that the peak level has the value 2; this normalization allowed us to avoid unrealistically high values for the [PhoP-P] interval in Fig. 3B and SI Fig. 6B, and unrealistically low values for K_2 and K_1^{dir} . The fitting method `ga` was empirically found to give better fits for the connector-mediated pathway model, while the method `fmincon` worked better for the direct regulation model. For the PmrD pathway model, we performed 10 fitting experiments and selected the best final fit. For the direct regulation model, we also performed 10 fitting experiments; the resulting fits gave parameter sets quite similar to each other, so we randomly selected one of them to be the final fit. At the randomized stage of our fitting procedure, the fitting routine was initialized with 20 different parameter sets, in which some of the parameters were selected at random. At the initial value adjustment stage, we performed 15 nonrandomized fitting–adjustment iterations.

In the fitting procedure for the direct regulation model, we used the condition that the depletion rate $k_{-1}^{dir} \geq 0.0154$, where 0.0154 corresponds to cell growth rate with doubling time 45 min. In the fitting procedure for the connector-mediated pathway, we assumed that $k_4 \gg k_{23}$, and $k_{-3} \gg k_3$. We thus chose $k_4 = 100$, $k_{23} = 1$, $k_{-3} = 50$, $k_3 = 0.1$; these values were neither randomized nor modified in the process of fitting. Other fixed values were $k_2 = 5$, $k_{-1}^{indir} = 0.2$. To

estimate k_2 (PmrD translation rate under full activation), we used the data from ref. 26 according to which the average time between two consecutive translation initiation events on one mRNA molecule is 2 s, which gives the initiation rate $1/2 \text{ s} = 30 \text{ min}^{-1}$; it is also known that translation initiation rates vary by several orders of magnitude (27). The estimate for k_{-1}^{indir} (mRNA degradation rate) was based on the article (28), which states that 80% of *E. coli* mRNA have half-lives between 3 and 8 min (exponential decay rate 0.2 min^{-1} corresponds to the half-life of ~ 3.5 min); in general, mRNA half-lives vary from 40 s to 20 min (29).

After fitting the connector-mediated pathway model (SI Eqs. 1–4) to the experimental data in Fig. 3A and generating Fig. 3B, we used the obtained parameter values to generate analogous curves for the PmrD regulation model with formation of active heterodimer (PmrA-P and PmrD/PmrA-P) (SI Eqs. 2–5). The difference between these curves and the curves in Fig. 3 was negligible, which suggests that heterodimer formation does not play an important role in the connector-mediated pathway dynamics.